



This is the accepted manuscript made available via CHORUS, the article has been published as:

Experimental demonstration of a photonic Aharonov-Bohm effect at radio frequencies

Kejie Fang, Zongfu Yu, and Shanhui Fan

Phys. Rev. B **87**, 060301 — Published 15 February 2013

DOI: [10.1103/PhysRevB.87.060301](https://doi.org/10.1103/PhysRevB.87.060301)

Experimental Demonstration of a Photonic Aharonov-Bohm Effect at Radio Frequency

Kejie Fang,¹ Zongfu Yu,² and Shanhui Fan²

¹*Department of Physics, Stanford University, Stanford, California 94305, USA*

²*Department of Electrical Engineering, Stanford University, Stanford, California 94305, USA*

Building upon recent theoretical proposals of creating effective gauge field for photons, we experimentally demonstrate the photonic Aharonov-Bohm effect. The effect relies on the non-reciprocal phase acquired by photons during photonic transitions. Our photonic Aharonov-Bohm interferometer is broadly tunable with a contrast ratio above 30 dB, as the operating frequency varies between 8–12 MHz.

While gauge field is only associated with charged particles in Nature, there are significant interests in achieving artificial gauge field for neutral particles [1]. This artificial gauge field can induce novel phenomena for neutral particles, such as quantized vortices [2] and quantum Hall effect [3], which originally can only exist in charged systems. For photons, in particular, achieving an artificial gauge field will lead to new mechanisms for controlling the flow of electromagnetic waves [4–8].

The hallmark of a gauge field is the Aharonov-Bohm effect [9, 10], which has been discovered initially for electronic systems under a magnetic field [11–13], and has subsequently been generalized to electrons in graphene under a strain field [14], and for gravity [15]. In the electronic Aharonov-Bohm effect, an electron propagating in the presence of a gauge field $\vec{A}(\vec{r})$ acquires an extra phase $\frac{e}{\hbar} \int \vec{A} \cdot d\vec{r}$, where the line integral occurs along the electron trajectory. This phase is non-reciprocal: reverting the propagation direction of the electron changes the sign of this phase. Also, this phase depends on the gauge choice and is not in itself an observable. However, phase difference between two different pathways is observable and thus can be detected by an interferometer. The response of the Aharonov-Bohm interferometer is non-reciprocal and depends on the direction of propagation.

To demonstrate a gauge potential for photons, it is therefore important to observe the photonic Aharonov-Bohm effect. Recently, it was shown theoretically that by controlling the phase of dynamical modulation of the dielectric constant of certain photonic systems [16–19], one can create an effective gauge field for photons [7, 8]. As a consequence, a photonic Aharonov-Bohm effect can be realized. In this Letter, we report the first experimental demonstration of the photonic Aharonov-Bohm effect.

We briefly review the theoretical proposal [7, 8] for creating an effective gauge field for photons. We consider a photonic structure supporting two photonic modes with frequencies ω_1 and ω_2 ($\omega_1 > \omega_2$). By modulating some aspects of the system such as its dielectric constant in time, one can induce a photonic transition between these two modes [16–21]. The transition process can be described by the coupled mode equation

$$i \frac{d}{dt} \begin{pmatrix} a_1 \\ a_2 \end{pmatrix} = \begin{pmatrix} \omega_1 & V \cos(\Omega t + \phi) \\ V \cos(\Omega t + \phi) & \omega_2 \end{pmatrix} \begin{pmatrix} a_1 \\ a_2 \end{pmatrix}, \quad (1)$$

where a_i is the amplitude of the i -th mode, and V , Ω , ϕ are the modulation strength, frequency and phase, respectively. We choose Ω be on resonance, i.e. $\Omega = \omega_1 - \omega_2$, and assume rotating wave approximation, which is valid when

$V \ll \Omega$. Transferring to the rotating frame ($a_i = e^{-i\omega_i t} \tilde{a}_i$), Eq. (1) becomes

$$i \frac{d}{dt} \begin{pmatrix} \tilde{a}_1 \\ \tilde{a}_2 \end{pmatrix} = \begin{pmatrix} 0 & \frac{V}{2} e^{-i\phi} \\ \frac{V}{2} e^{i\phi} & 0 \end{pmatrix} \begin{pmatrix} \tilde{a}_1 \\ \tilde{a}_2 \end{pmatrix}. \quad (2)$$

From Eq. (2), it is apparent that a photon making a transition from a low frequency mode to a high frequency mode acquires a phase $-\phi$, while it acquires a phase ϕ if it makes a transition from a high frequency mode to a low frequency mode.

The modulation phase here corresponds to a gauge potential for photons [7]. Corresponding to the photonic transition between the two states $|1\rangle$ and $|2\rangle$ as described in Eqs. (1) and (2), we can define an effective gauge field A_{eff}

$$\int_1^2 A_{\text{eff}} \cdot d\vec{l} = \phi. \quad (3)$$

In the definition of Eq. (3), we imagine the integration to be along a pathway that connects the states $|1\rangle$ and $|2\rangle$ in a parameter space. In the case where $|1\rangle$ and $|2\rangle$ are spatially separated, such a definition directly leads to a gauge potential in real space and hence an effective magnetic field for photons [8]. The definition here however is more general.

We see that A_{eff} defined in this way satisfies all the requirements for a gauge potential. It induces a non-reciprocal phase since reverting the direction of integral in Eq. (3), i.e. reverting the direction of the photonic transition, changes the sign of the phase. Also, similar to the electronic gauge potential, A_{eff} here exhibits a gauge degree of freedom or gauge ambiguity, since the definition of the modulation phase depends on a choice of time-origin which is completely arbitrary [7]. However, the phase difference between two different pathways is gauge invariant, and detecting such a phase difference induced by a gauge degree of freedom lies at the heart of the Aharonov-Bohm effect.

Our experimental setup for demonstrating the photonic Aharnov-Bohm effect is a two-arm interferometer schematically shown in Fig. 1a. A corresponding photo of the setup, with details of various components used, is provided in Fig. 1b. The lower arm consists of a voltage variable attenuator that controls the amplitude attenuation, and a voltage variable phase shifter that controls the phase delay. The upper arm consists of two mixers separating a sequence of three filters. The two mixers are driven by a same signal generator. The setup is identical for the left- and right-propagation directions.

In this setup, the mixers provide the photonic transition and generate the effective gauge potential. For an input wave having a form $\cos(\omega't)$, the mixer multiplies it with a local oscillator $\cos(\Omega t + \phi)$, the resulting output wave is

then proportional to

$$\cos(\omega't)\cos(\Omega t + \phi) = \frac{1}{2}\cos(\omega't + \Omega t + \phi) + \frac{1}{2}\cos(\omega't - \Omega t - \phi). \quad (4)$$

We therefore see that through the mixer, the upward transition $\omega' \rightarrow \omega' + \Omega$ and the downward transition $\omega' \rightarrow \omega' - \Omega$ both carry a phase that is equal to the local oscillator phase in magnitude but opposite in sign.

The input wave has a frequency ω near ω_0 . The filters at the ends of the upper arm allow high transmission near ω_0 while suppressing transmission near $\omega_0 + 2\Omega$. The filter in the middle allows transmission near $\omega_0 + \Omega$ while suppressing transmission near $\Omega - \omega_0$. Thus the combination of the mixers and filters results in a photonic transition sequence where a photon, initially at a state $|1\rangle$ with a frequency ω , makes a transition to a state $|2\rangle$ with a frequency $\Omega + \omega$, and then makes another transition back to the state $|1\rangle$.

We choose the phase of the local oscillators at the two mixers to be $\phi(z_1)$ and $\phi(z_2)$, respectively. As noted above in Eqs. (1) to (3), these phases are related to an effective gauge field for photons. Also, each phase $\phi(z_1)$ or $\phi(z_2)$ is “gauge-dependent”. It depends on the choice of time-reference and hence can be arbitrarily chosen. However, the phase *difference* between the local oscillators of the two mixers, i.e. $\phi(z_1) - \phi(z_2)$, is gauge-independent and thus observable. Thus, the interferometer here provides a precise photonic analogue of the electronic Aharonov-Bohm effect: it detects a non-reciprocal phase corresponding to a gauge degree of freedom.

In our interferometer, for a right-propagating photon, the phase difference between the two arms is $\phi(z_1) - \phi(z_2) + \phi_{s2} - \phi_{s1}$, where ϕ_{si} are the free-propagation phase in the two arms. On the other hand, for a left-propagating photon, the phase difference between the two arms is $-\phi(z_1) + \phi(z_2) + \phi_{s2} - \phi_{s1}$. Note the sign difference of the accumulated phase due to the mixers: In the upper arm, the right-propagating photon goes through an upward transition at mixer 1 and then a downward transition at mixer 2, whereas the left-propagating photon goes through an upward transition at mixer 2 and a downward transition at mixer 1. The transmission amplitude of the interferometer for the two directions is thus

$$V \cos\left(\frac{\pm(\phi(z_1) - \phi(z_2)) + \phi_{s2} - \phi_{s1}}{2}\right), \quad (5)$$

where V is the maximum of the transmitted field amplitude. The transmission is non-reciprocal for a general choice of $\phi(z_1) - \phi(z_2)$.

To demonstrate the effect of the non-reciprocal phase, we fix $\phi_{s2} - \phi_{s1} = \pi/2$ by adjusting the phase shifter in the lower arm. We use an input signal with a frequency $\omega = 2\pi \times 10$ MHz. The local oscillators for the mixers have a

frequency $\Omega = 2\pi \times 60$ MHz. The transmitted field amplitude, measured as a function of $\phi(z_1) - \phi(z_2)$, is plotted in Fig. 2a. We observed the typical oscillation of transmission with varying gauge field (here through local oscillator phases) as in the Aharonov-Bohm effect. In particular, at $\phi(z_1) - \phi(z_2) = \pm\pi/2$, the two opposite propagations show near-complete contrast with a contrast ratio above 30 dB in power. The loss in the upper arm is limited by the conversion loss of the frequency mixer which is about 7 dB each.

The operating frequency of the device is completely tunable. In Fig. 2b, we conduct a sequence of experiments with continuous-wave input, where we change the frequency of the input wave. The local oscillator phases are maintained at $\phi(z_1) - \phi(z_2) = \pi/2$. For each input frequency, we re-adjust the phase shifter such that the condition $\phi_{s2} - \phi_{s1} = \pi/2$ is maintained. We see that the contrast ratio is independent of the operating frequency (Fig. 2b), with the contrast ratio between the forward and backward transmission maintained at near 32 dB over the frequency range of 8–12 MHz.

Around each operating frequency between 8–12 MHz, the operating bandwidth in our current setup is limited by the phase shifter which has a relatively narrow bandwidth. At a given center frequency ω , the tuning voltage of the phase shifter can be adjusted such that $\phi_{s2} - \phi_{s1} = \pi/2$, resulting in a near-ideal contrast between the forward and backward direction at that frequency, as demonstrated above. However, away from the center frequency ω , without readjusting the phase shifter, the condition $\phi_{s2} - \phi_{s1} = \pi/2$ is no longer satisfied, resulting in a degradation of the contrast ratio which limits the operating bandwidth of our interferometer. As an illustration of this effect, Fig. 2c presents a sequence of experiments around a center frequency of $\omega = 2\pi \times 10$ MHz, with the phase shifter tuned such that near-ideal contrast is obtained at this frequency. In this experiment, we again vary the input frequency as we have done for the experiment shown in Fig. 2b. However, here at each input frequency we no longer adjust the phase shifter. The contrast ratio in this case indeed degrades as we change the operating frequency. We observe, however, significant contrast over the entire frequency range of 8–12 MHz, with the contrast ratio above 10 dB over the frequency range of 8 – 10.4 MHz, indicating the existence of substantial operating bandwidth in this device. Further improvement of the operating bandwidth can be accomplished by operating in the GHz frequency range where broad-band phase shifter is available.

Our experiment here provides a broadly-tunable and linear isolator without the use of Ferrite. We note that demonstrating such non-magnetic isolator is of significant practical importance in micro-wave domain [22–24]. In contrast to the experiments in Ref. [23] and [24], which used the nonlinear current-voltage relation of an electrical

diode to achieve non-reciprocity for electromagnetic waves, the construction here is completely linear with respect to the amplitude of the input electromagnetic wave. Also, the bandwidth of the interferometer is in principle broader as resonance effect is not necessary in our device. One could also envision demonstrating similar effect in the optical wavelength range [7, 8], as dynamic modulation in the optical domain is becoming readily achievable [17, 20, 21, 25, 26]. The demonstration of effective gauge fields for photons may lead to a new set of techniques for manipulating electromagnetic wave.

ACKNOWLEDGEMENTS

This work is supported in part by U. S. Air Force Office of Scientific Research grant No. FA9550-09-1-0704, and U. S. National Science Foundation grant No. ECCS-1201914.

-
- [1] For a review, see J. Dalibard, F. Gerbier, G. Juzeliunas, and P. Ohberg, *Rev. Mod. Phys.* **83**, 1523 (2011).
- [2] Y.-J. Lin, et. al., *Nature* **462**, 628 (2009).
- [3] A. S. Sørensen, E. Demler, and M. D. Lukin, *Phys. Rev. Lett.* **94**, 086803 (2005).
- [4] M. Hafezi, E. A. Demler, M. D. Lukin, and J. M. Taylor, *Nature Phys.* **7**, 907 (2011).
- [5] R. O. Umucallar and I. Carusotto, *Phys. Rev. A* **84**, 043804 (2011).
- [6] J. Koch, A. A. Houck, K. Le Hur, and S. M. Girvin, *Phys. Rev. A* **82**, 043811 (2010).
- [7] K. Fang, Z. Yu, and S. Fan, *Phys. Rev. Lett.* **108**, 153901 (2012).
- [8] K. Fang, Z. Yu, and S. Fan, *Nature Photonics* **6**, 782 (2012).
- [9] W. Ehrenberg and R. E. Siday, *Proc. Phys. Soc. London Sect. B* **62**, 8 (1949).
- [10] Y. Aharonov and D. Bohm, *Phys. Rev.* **115**, 485491 (1959).
- [11] A. Tonomura, et. al., *Phys. Rev. Lett.* **56**, 792 (1986).
- [12] R. A. Webb, S. Washburn, C. P. Umbach, and R. B. Laibowitz, *Phys. Rev. Lett.* **54**, 2696 (1985).
- [13] A. Bachtold, et. al., *Nature* **397**, 673 (2009).
- [14] F. de Juan, A. Cortijo, M. A. H. Vozmediano, and A. Cano, *Nature Physics* **7**, 810 (2011).
- [15] L. H. Ford and A. Vilenkin, *J. Phys. A: Math. Gen.* **14**, 2353 (1981).
- [16] J. N. Winn, S. Fan, J. D. Joannopoulos, and E. P. Ippen, *Phys. Rev. B* **59**, 1551 (1999).
- [17] P. Dong, S. F. Preble, J. T. Robinson, S. Manipatruni, and M. Lipson, *Phys. Rev. Lett.* **100**, 033904 (2008).
- [18] Z. Yu and S. Fan, *Nature Photon.* **3**, 91 (2009).
- [19] Z. Yu and S. Fan, *Appl. Phys. Lett.* **94**, 171116 (2009).
- [20] H. Lira, Z. Yu, S. Fan, and M. Lipson, *Phys. Rev. Lett.* **109**, 033901 (2012).
- [21] D. M. Beggs, et al., *Phys. Rev. Lett.* **108**, 213901 (2012).
- [22] A. Kamal, J. Clarke, and M. H. Devoret, *Nature Phys.* **7**, 311 (2011).
- [23] T. Kodera, D. L. Sounas, and C. Caloz, *App. Phys. Lett.* **99**, 031114 (2011).
- [24] Z. Wang, et. al., *PNAS* **109**, 13194 (2012).
- [25] Q. Xu, B. Schmidt, S. Pradhan, and M. Lipson, *Nature* **435**, 325-327 (2005).
- [26] Y. -H. Kuo, et al., *Nature* **437**, 1334-1336 (2005).

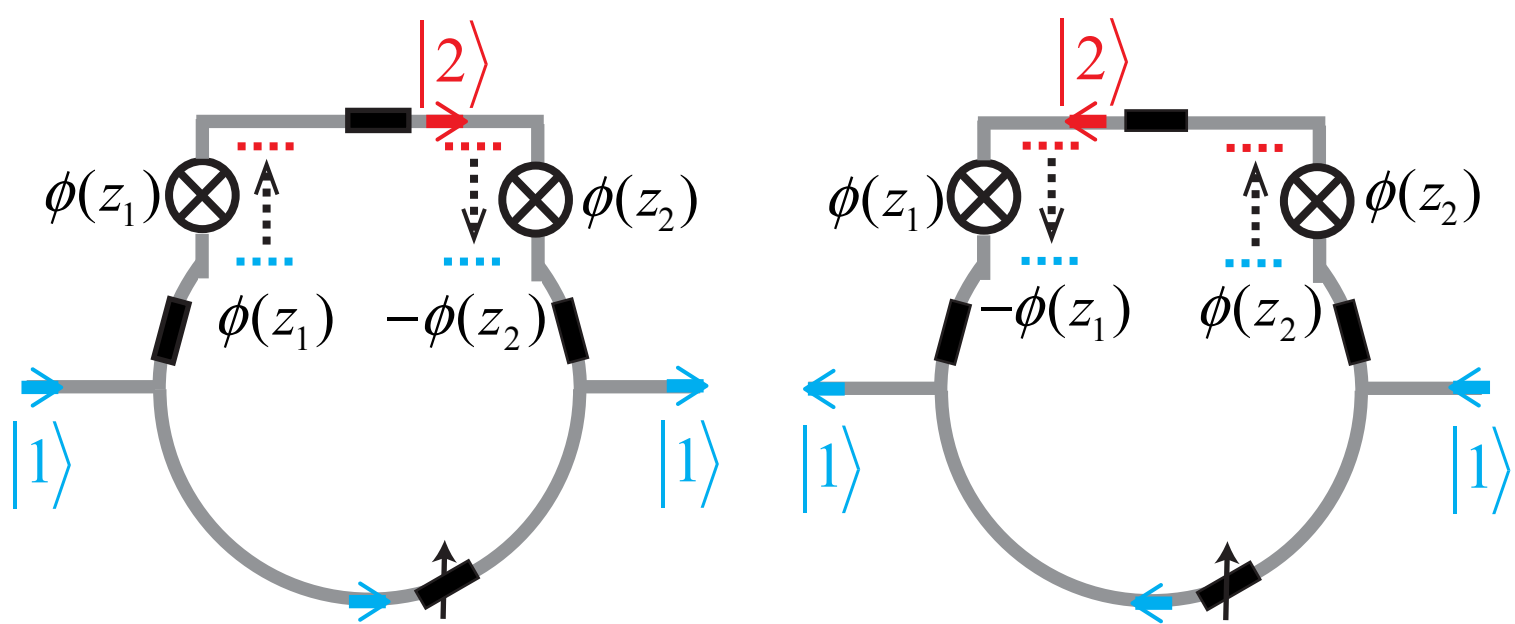
FIGURES

FIG. 1: **a** Schematics for the demonstration of a photonic Aharonov-Bohm effect. The signal of the two local oscillators with the mixers are provided by a same signal generator but with phase $\phi(z_1)$ and $\phi(z_2)$, respectively. Dashed lines and arrows represent photonic transition between $|1\rangle$ at frequency ω and $|2\rangle$ at frequency $\Omega + \omega$ induced by mixers. Circle with cross: mixer; black rectangle: filter; black rectangle with arrow: tunable attenuator and phase shifter.

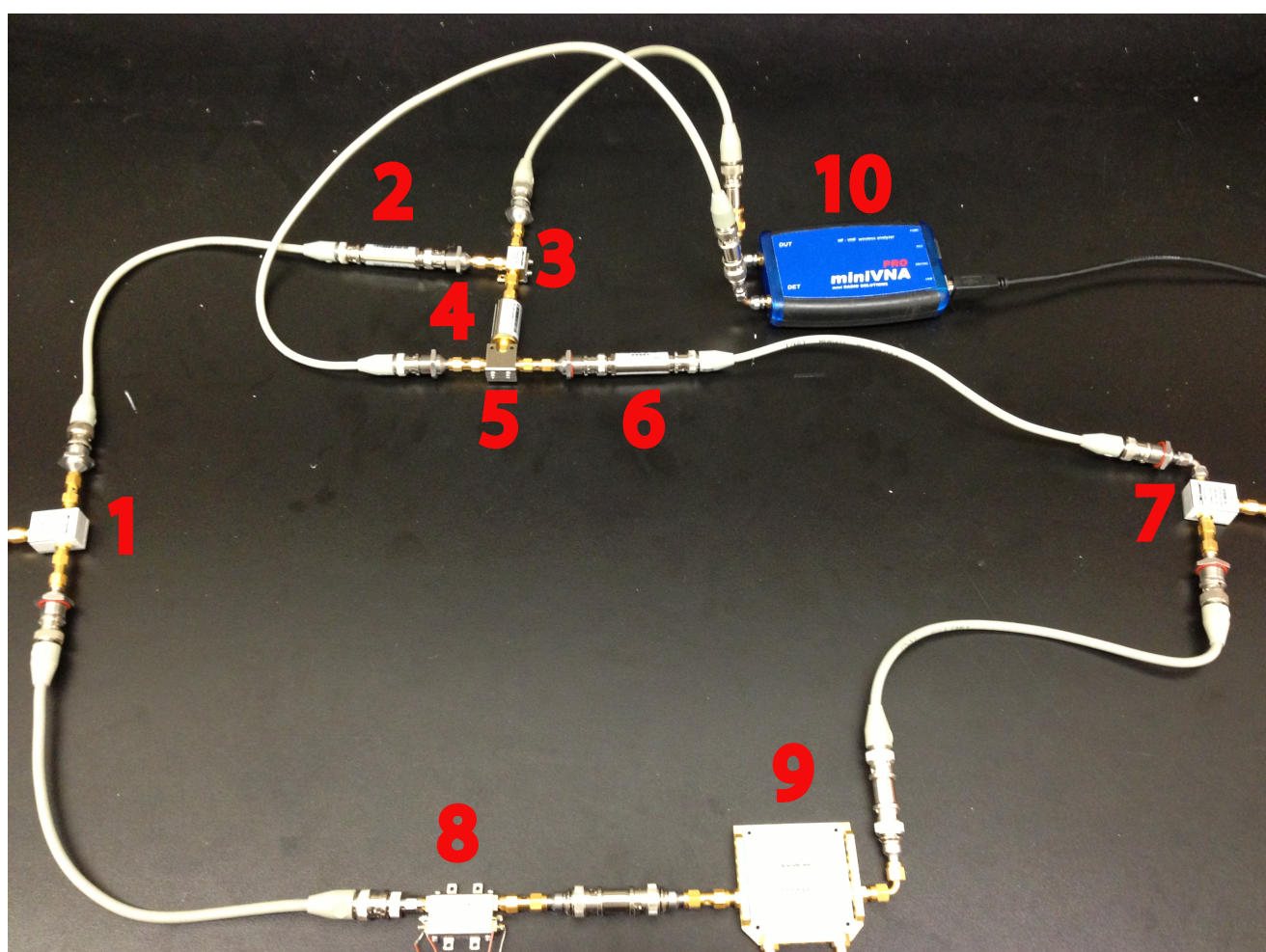
b Experimental setup. 1, 7: 50/50 power splitter/combiner (Mini-Circuits ZFRSC-123). 3, 5: Frequency mixer (Mini-Circuits ZX05-10L). 4: Bandpass filter (Mini-Circuits SBP-70, with a passband of 63-77 MHz). 2, 6: Lowpass filter (Mini-Circuits BLP-21.4, with a passband from DC to 22 MHz). 8: Voltage variable attenuator (Mini-Circuits ZX73-2500). 9: Voltage variable phase shifter (Mini-Circuits JSPHS-12, with an operating bandwidth of 8-12 MHz). 10: Vector network analyser (served as the driver for the local oscillators of the mixers).

FIG. 2: **a** Transmitted field amplitude as a function of $\phi(z_1) - \phi(z_2)$ for photons propagating to right (blue) and left (red), respectively. The input is at a frequency of 10 MHz. Solid lines are fitted curves using Eq. (5). **b** Contrast ratio between forward and backward directions as a function of operating frequency. At each frequency, we readjust the phase shifter such that $\phi_{s2} - \phi_{s1} = \pi/2$. **c** Same as **b**. Except the phase shifter is chosen to maximize the contrast ratio for a frequency near 10 MHz, and is not re-adjusted as we vary the operating frequency.

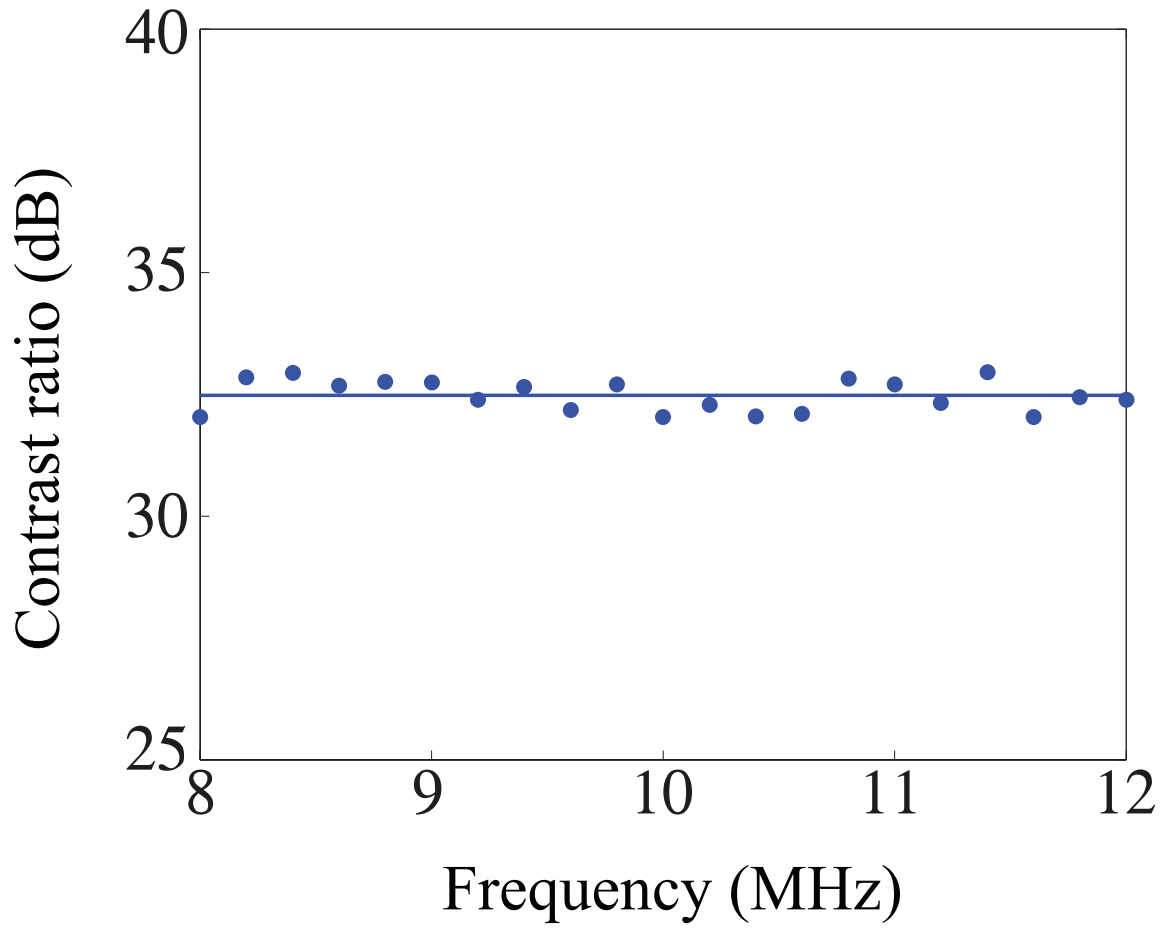
a



b



$$\phi(z_1) - \phi(z_2)$$

b**c**